Influence of the Spark Plasma Sintering temperature on the structure and dielectric properties of $BaTi_{(1-x)}Zr_xO_3$ ceramics

Blessing N. Ezealigo[1], Roberto Orrù[1,*], Catherine Elissalde[2,*], Hélène Debéda[3], U-Chan Chung[2], Mario Maglione[2], Giacomo Cao[1]

[1]*Dipartimento di Ingegneria Meccanica, Chimica e dei Materiali, Unità di Ricerca del Consorzio Interuniversitario Nazionale per la Scienza e Tecnologia dei Materiali (INSTM) - Università degli Studi di Cagliari, via Marengo 2, 09123 Cagliari, Italy*

[2]*Université de Bordeaux, CNRS, ICMCB, UMR 5026, 87 avenue du Dr A. Schweitzer, 33608 Pessac, France*

[3]*Université de Bordeaux, Laboratoire IMS, UMR 5218, 351 Cours de la Libération, 33405 Talence, Cedex, France*

(*) Author to whom all correspondence should be addressed

https://doi.org/10.1016/j.ceramint.2020.09.210

July 2020

Abstract

Structural and dielectric properties of $BaTi_{(1-x)}Zr_xO_3$ (BTZ) ceramics prepared by Spark Plasma Sintering (SPS) from powders obtained via Self-propagating High-temperature Synthesis (SHS) are shown in this work to be strongly affected by the sintering temperature. In addition, a post-annealing treatment in air of the as-prepared ceramics leads to a transition from the hexagonal to the tetragonal and cubic phases. The SPS ceramics corresponding to compositions $0.05 \leq x \leq 0.20$ and obtained at a sintering temperature of 1200°C exhibit a standard ferroelectric behavior. In contrast, a diffuse phase transition is observed for ceramics sintered at higher temperatures. Finally, the BTZ ceramic containing 5 at.% of Zr displays the best dielectric permittivity and piezoelectric properties as compared to the other compositions taken into account.

Keyword: Dielectric permittivity, spark plasma sintering, piezoelectric, post-annealing; self-propagating high-temperature synthesis.

Corresponding authors: roberto.orru@dimcm.unica.it, catherine.elissalde@icmcb.cnrs.fr

1. Introduction

To meet specific applications, the strategy commonly adopted by the scientific community to improve the electrical characteristics of ABO_3 perovskite materials is to change the chemical content of the ceramics. Indeed, the substitution of the A or B cation sites with other isovalent ions can modify the dielectric properties of the material, and also lead to changes in the related transition temperatures as well as the formation of specific phases **[1]**. In this context, zirconium substituted barium titanate (BTZ) has attracted great attention in the last decade because of its wide range of applications, owing to its improved properties and potential to replace lead-based ferroelectric materials **[2-3]**. These properties include high dielectric permittivity, relatively low dielectric loss, large voltage tunability of the dielectric permittivity, good chemical stability, and attractive lead-free relaxor behavior **[4-6]**.

In this regard, various authors have reported on the marked influence of the substitution with Zr in Ti site of $BaTiO_3$ on the properties of the BTZ ceramics obtained by conventional sintering **[7-9]**. The potential of BTZ for application in tunable microwave devices has been demonstrated **[10]**. Specifically, it is reported that, when the amount of Zr content is within the range $0 \leq x \leq 0.10$, the ceramics show a classical ferroelectric behavior **[9, 11]**. However, at higher Zr content, the ferroelectric phase coexists with the paraelectric one, leading to a diffuse phase transition. The latter one is promoted by the energy difference between the ferroelectric and the paraelectric phases **[12]**. Furthermore, the classical ferroelectric transitions of $BaTiO_3$ continuously give rise to diffuse phase transition ($0.10 < x \leq 0.26$) and relaxor state ($0.26 < x \leq 0.40$), whose temperature of occurrence decreases to low values as the Zr content increases **[13]**. It is worth to mention that, in addition to the latter finding, the phase transition can also be influenced by temperature variation, depolarization due to presence of porosity, slight changes in

the chemical potential, and grain size effect **[12, 14-15]**. A high dielectric permittivity of about 14,000 has been reported for dense BTZ ceramics (x=0.08), which was obtained by solid state reaction using high energy milling followed by conventional sintering **[9]**.

Among the synthesis methods proposed for obtaining BTZ powders, Sol-gel **[16-17]**, Sol-gel based Pechini method **[18]**, solid-state reactions **[19-20]**, and combustion synthesis **[21-22]** are reported. The formation of BTZ solid solution is obtained by conventional sintering in the temperature range 1300−1450°C after 2−10h treatment. In addition to conventional sintering, only few studies have also been conducted on BTZ ceramics using Spark Plasma Sintering (SPS) **[23-25]**. SPS is an efficient sintering process where powders are rapidly heated by Joule effect due to the combination of pulsed electric current and the application of uniaxial mechanical pressure **[26]**. In particular, the structure and electromechanical properties of $Ba(Zr_{0.2}Ti_{0.8})O_3$ ceramics obtained by SPS at 1100°C and subsequently annealed at 1000−1400°C for 12h has been investigated by Maiwa **[23, 27]**.

In this work, the Self-propagating high-temperature synthesis (SHS) and Spark Plasma Sintering techniques are combined for the first time for the preparation of barium titanate ($BaTi_{(1-x)}Zr_xO_3$) ceramics with different Zr concentrations. Briefly, SHS is a combustion synthesis method based on the local ignition of highly exothermic reactions which can self-propagate without additional energy supply **[28-29]**. Temperatures in the range 2000−5000 K and cooling rates up to 10^3 K/min can be reached during SHS and, more importantly, high-purity products can be correspondingly obtained in a very short time (order of seconds) **[28]**.

The present work is aimed to produce single-phase $BaTi_{(1-x)}Zr_xO_3$ (x=0.05−0.25) ceramics by combining the two fast processes mentioned above, i.e. through the so-called SHS-SPS approach. The influence of the sintering temperature (T_D) on the density, composition (structure),

dielectric, and piezoelectric properties of the SHS-SPS ceramics is systematically investigated. The optimal SPS, as well as post-annealing, conditions, are then identified. We present a novel procedure of tuning the dielectric response of the BTZ ceramics by varying the sintering temperature regardless of the Zr content.

2. Experimental

BTZ powders were prepared by SHS according to the following chemical equation:

$$2BaO_2 + (1-2x)TiO_2 + 2xZrO_2 + Ti \rightarrow 2BaTi_{(1-x)}Zr_xO_3 \quad (1)$$

Hereto after, the $BaZr_{0.05}Ti_{0.95}O_3$, $BaZr_{0.10}Ti_{0.90}O_3$, $BaZr_{0.15}Ti_{0.85}O_3$, $BaZr_{0.20}Ti_{0.80}O_3$, and $BaZr_{0.25}Ti_{0.75}O_3$ compositions will be indicated as BTZ005, BTZ010, BTZ015, BTZ020, and BTZ025, respectively. Details on the synthesis of the precursors and procedure can be found in **[30]**.

The SHS products were first converted into powders after 20 min ball milling treatment using a SPEX 8000 mixer mill (SPEX CertiPrep, Metuchen, NJ, USA). Subsequently, 3g of the resulting powders were consolidated by spark plasma sintering (515S model, Fuji Electronic Industrial Co., Ltd., Kanagawa, Japan) under vacuum conditions (down to 20 Pa) and sintering temperatures (T_D) in the range 1200–1400 °C (heating rate of 100°C/min and holding time of 5 min) with a mechanical pressure of 40 MPa. Graphite die of 14.7 mm inner diameter, 30 mm height, and 30 mm outer diameter was used. SPS runs were carried out under temperature-controlled mode using an optical pyrometer (IR-AHS2, Chino, Tokyo, Japan) focused on the external surface of the die. After SPS, the bulk samples were polished on their top and bottom surfaces using progressively finer abrasive paper, to finally obtain 2 mm thick disks. The pellets were then post annealed for 3h at 1200°C (Nabertherm, mod. N60/ER, Germany) in an oxygen-

rich atmosphere to re-oxidize the samples and remove the carbon contamination arising from the graphite tools.

The absolute density values of the bulk specimens were determined by the Archimedes' method using distilled water as immersion medium. The crystalline phases in both the SHS powders and the SPS specimens were identified using an X-ray diffractometer (PANalytical X'pert Pro diffractometer, Netherlands; operating at 40 kV and 40 mA, using the X'Celerator detector) equipped with a Ni filtered CuKα radiation (λ = 1.5405 Å).

Fracture surfaces of BTZ ceramics were examined by high resolution scanning electron microscopy (HRSEM) (mod. S4000, Hitachi, Tokyo, Japan) equipped with a UltraDry EDS Detector (Thermo Fisher Scientific, Waltham, MA, USA). Microstructural analysis (grain size, porosity) were conducted on SEM images using the open source software Image J (version 1.54a for Windows, 64 bit, National Institutes of Health, Bethesda, MD, USA).

The dielectric measurements were carried out after depositing by sputtering gold electrodes on both sides of the dense ceramics (Technics Hummer JR, USA). The LCR meter (Wayne Kerr 4300, London) recorded the capacitance and imaginary permittivity (ε_i) values from which the data acquisition program estimated the dielectric permittivity and dielectric loss. Liquid nitrogen was used to decrease the temperature of the set up to about 85 K and a furnace (Eurotherm 3508, UK) raised the temperature to 450K which was measured using a K-type thermocouple. For the sake of reproducibility, each experiment was repeated at least twice.

Regarding the measurement of the piezoelectric properties, the samples were poled at a high voltage of about 2 kV (10 kV/cm) generated by a suitable supply (AET technologies, France) at 80°C under Nitrogen gas in a furnace (AET technologies, France). The applied field was kept during sample's cooling. The resonance (f_r) and anti-resonance (f_a) frequencies from which the

electromechanical parameters were estimated, have been obtained using a network analyzer (Agilent technologies E5061B, USA).

3. Results

3.1 SHS powders of Zr substituted $BaTiO_3$

The five BTZ compositions investigated in the present work all display a self-propagating character, i.e. the reaction occurred spontaneously after initiation without additional energy, regardless of the Zr content. The XRD patterns of the resulting SHS products, after being milled to powders, are shown in **Fig. 1.**

The hexagonal $BaTiO_3$ phase is the only one (matched with the JCPDS card reference pattern mentioned in **Fig. 1**) detected by this analysis for x=0.05 and 0.10. Also, some peaks identified as *c* $BaZrO_3$ and *t* BTZ appear in the XRD patterns of SHS products obtained for larger Zr content (x>0.10). Moreover, their intensity, and in particular that of the peak corresponding to the cubic $BaZrO_3$ phase, progressively increases as the x value is augmented. It is important to note that in the powders synthesized by SHS, the desired single phase BTZ was not achieved (**Fig. 1**), rather an additional $BaZrO_3$ phase was formed, which implies that at this stage Zr is yet to be fully substituted in the B site of the $BaTiO_3$ lattice.

3.2 Spark Plasma Sintering of SHS powders

The powders synthesized by SHS were then processed by SPS (5 min, 40 MPa, 100°C/min). The influence of the sintering temperature on the composition can be observed from room temperature XRD results depicted in (**Fig. 2)**. Specifically, the XRD patterns of the bulk samples for the five BTZ systems are compared in **Fig. 2(a)-(b)** for two selected sintering

temperatures 1200°C and 1400°C, respectively. It is important to note that XRD data for Zr-substituted $BaTiO_3$ powders sintered at T_D=1300°C are very similar to those obtained at 1400°C, hence they are not reported here.

The XRD patterns evidence that, regardless of the Zr content, the *h* $BaTiO_3$ originally present in SHS powders undergoes a gradual structural (phase) transformation during SPS. Specifically, this effect is more pronounced as the dwell temperature is increased from 1200 to 1400°C. Nonetheless, when considering the composition corresponding to x=0.05, the original hexagonal phase is still significantly present in the sintered ceramic. A direct indication of the phase transformation observed when x increases is provided, for example, by the intensity of the *h* $BaTiO_3$ peak which falls in the range $26° \leq 2\theta \leq 27°$. This peak decrease and tends to disappear, particularly when T_D=1400°C. The XRD analysis also evidences that, when the sintering process is performed at 1400°C, the intensity of the *c* $BaZrO_3$ and the *h* $BaTiO_3$ peaks are also markedly reduced with respect to the starting SHS powders (**Fig. 1**). It is thus possible to conclude that, depending on the x value, the content of *t* BTZ or the *c* BTZ phases is enhanced **Fig. 2(b)**) during SPS when the sintering temperature is high enough. This is confirmed by the shift in 2θ diffraction peak at about 31° towards a lower angle (**Fig. 2(c)**). However, a residual presence of *c* $BaZrO_3$ is still detected by XRD. In the literature, the tetragonal phase is generally reported for $x \leq 0.08$ **[8, 31][31]** while the cubic and/or rhombohedral phases are found for $x \geq 0.10$ **[18, 20, 32-33]**.

3.3 Post-annealing of SPS samples

From the results described in *section 3.2*, it is found that the bulk specimens obtained by SPS still contain undesired secondary phases, particularly *h* $BaTiO_3$ and/or *c* $BaZrO_3$, whatever the Zr content. The effect of a post-heat treatment in air, conducted for 3 h at 1200°C, on the

composition of the BTZ ceramics produced by SPS at T_D= 1200, 1300, and 1400°C, was then investigated. The room temperature XRD patterns of the corresponding post-annealed samples are shown in **Fig. 3(a)-3(b)**, for the compositions corresponding to x=0.05 and 0.25, i.e. the lowest and highest Zr content examined in this work.

Let's consider first the ceramics obtained with the lowest Zr content (**Fig. 3(a)-3(b))**. The post-annealing treatment appears to remove the *h* $BaTiO_3$ phase initially present in SPS sintered products (**Fig. 2(a)-2(b)**). Also, *t* BTZ is the major phase detected by XRD at room temperature in post-thermal treated SPS ceramics obtained at T_D=1200 and 1300°C. On the other hand, both *h* $BaTiO_3$ and *t* BTZ present in the sintered ceramics produced at 1400°C (**Fig. 2(b))** are transformed into *c* BTZ. The latter one is the major phase in the product, with a lower amount of residual *t* BTZ, for x=0.05, as shown in **Fig. 3(b)**. The coexistence of phases could arise from the segregation of Zr when high sintering temperature (1400°C) is applied on heterogeneous starting powders. As a result, ceramics containing Zr rich (cubic) and Zr poor (tetragonal) parts could be obtained **[34]**).

XRD data of post-annealed SPS samples corresponding to x=0.25 are shown in **Fig. 3(c)**. Residual $BaZrO_3$ is reduced during post heat treatment in air, to finally provide single-phase *c* BTZ for ceramics processed by SPS at T_D=1400°C. It should be noted that the compositional changes observed when considering x=0.10, 0.15, and 0.20, not reported here for the sake of brevity, fall within those described above in the case of x=0.05 and 0.25.

Another effect observed after the post-annealing treatment is the change of color of the SPS samples. Indeed, as shown in **Fig. 4a**, after the sintering process, the resulting disks are dark. The post-annealing treatment performed at various temperatures/time conditions evidences that, at relatively lower temperatures (800–1000°C), the samples exhibited several cracks on their surface, and the transformation from dark to white color was not obtained. In contrast, such drawback was

avoided, or strongly limited, when the annealing process was conducted for 3 h at 1200°C. The optical images of the various BTZ samples correspondingly obtained are shown in **Fig. 4b**. The annealing process induces a significant color change from dark to white-grey in all BTZ ceramics. Thus, a post-annealing at 1200°C for 3h appears as the optimal condition to be adopted.

3.4 Microstructural characterizations

SEM images of the fracture surfaces of BTZ005 and BTZ025 ceramics obtained by SPS at T_D=1200 and 1400° and annealed at 1200°C for 3h are shown in **Fig. 5(a)-5(d)**. The densities of post-annealed ceramics are reported in **Fig. S1 (Suppl. material)**.

BTZ005 sintered at 1200°C exhibits an inhomogeneous microstructure with several dense zones made of grains with a melted aspect that make difficult an accurate evaluation of the corresponding grain size (**Fig.5a**). These areas are still present in ceramics sintered at 1400°C, while the microstructure is globally more homogeneous with well-defined grains and grain boundaries (**Fig.5b**). The observed transgranular fracture mode reflects weak grain boundaries. Grain size estimated using Image J software **[35]** is in the range 2–4 μm, so that no exaggerated grain growth is observed despite the high sintering temperature. The microstructure of BTZ025 ceramics sintered at 1200°C is characterized by a significant level of porosity and the presence of cracks (**Fig.5c**). This is in agreement with the low value of density obtained (**Fig. S1**). Similar to BTZ005, when the sintering temperature is increased up to 1400°C, the microstructure becomes denser, in good agreement with the values reported in **Fig. S1**. The fracture remains transgranular and equiaxed grains in the size range 1–3 μm are observed.

3.5 Dielectric study

3.5.1 Effect of sintering temperature on dielectric behavior

The variation of the dielectric permittivity as a function of temperature for the BTZ ceramics sintered at different T_D and post-annealed for 3h at 1200ºC are shown in **Fig. 6.**

For a fixed composition, both the permittivity values and the transition temperatures are affected by the sintering temperature. Higher T_D leads to a decrease of the temperature corresponding to the maximum of permittivity value (T_m) as well as an increase in permittivity levels, especially in the vicinity of the transition (**Fig. 7; Table S1 (Suppl. Material**)). In particular, it is worth noting that for the composition corresponding to x= 0.05, an increase of the sintering temperature from 1200°C to 1400°C induces also a change from a classical ferroelectric to a more diffuse phase transition. A decrease of the Curie Temperature and an increase of the Rhombohedral (R)−Orthorhombic (O) [R−O] and Orthorhombic (O)−Tetragonal (T) [O−T] phase transitions were correspondingly observed. When the Zr content is increased, the transition temperature is decreased, as expected, and for ceramics sintered at temperatures higher than 1200°C, the ferroelectric behavior changes from classical (x=0.05) to a diffuse mode (x>0.10). The dielectric study as a function of temperature (**Fig. 6**) confirms the diffuse (not relaxor) behavior of the BTZ ceramics obtained by SHS-SPS, due to the absence shift in T_m as a function of frequency for 0.05≤x<0.20 (**Fig. S2 (Suppl. Material))**. Whatever the Zr content and the sintering temperature, the dielectric loss at 1 kHz remains stable and mostly lower than 8%. The comparison of dielectric behavior with regards to T_D for each Zr composition is shown in **Fig. S3 (Suppl. Material)**.

To investigate the behavior in the paraelectric region, the Curie constant, C, was estimated from the Curie-Weiss law:

$$\varepsilon = \frac{C}{(T - T_o)}; (T>T_c) \qquad (2)$$

where T_c is the Curie point (transition temperature).

The inverse of the dielectric permittivity (1/ε) plotted as a function of temperature was used to estimate the Curie-Weiss temperature (T_o) and the Curie constant **Fig. 8** and **Table S2 (Suppl. Material).**

Regarding the investigated range of Zr content, the Curie constant decreases monotonically with an increase of the *x* value for a given T_D. Also, the Curie-Weiss temperature was found to decrease with T_D and Zr content.

The modified Curie-Weiss (C-W) plot can be used to describe the deviation from linearity due to the diffuse character of the transition. The modified Curie-Weiss equation is given by:

$$\frac{1}{\varepsilon} - \frac{1}{\varepsilon_m} = \frac{(T - T_m)^\gamma}{C}\ ;\ (T>T_m) \qquad (3)$$

where ε is the real permittivity, ε_m is the maximum dielectric constant, T_m is the temperature at the maximum dielectric permittivity, γ is the diffuseness coefficient. For normal ferroelectrics γ=1, while for relaxor γ=2.

The modified Curie-Weiss plots and the corresponding data are provided in **Fig. S4** and **Table S2 (Suppl. Material)**, respectively.

To illustrate the change of behavior from classical to diffuse one as a function of the Zr content, the variation of T_c (T_m) and diffuseness coefficient are presented in **Fig. 9** for ceramics sintered at 1400°C.

3.6 Piezoelectric study

In **Fig. 10** the results of the piezoelectric study of BTZ are presented. The piezoelectric charge coefficient (d_{31}) and the planar electromechanical coupling factor (k_p) were significantly

influenced by the SPS temperature (T_D). All samples show good mechanical quality factor (Q_m), consistent with the low dielectric loss (**Table S3 (Suppl. Material))**. The resonance-antiresonance measurement for BTZ005 ceramics sintered at 1300℃ is shown in **Fig S5 (Supp. Material**). BTZ025 samples could not be poled due to high current leakage arising from their low density. Hence, no piezoelectric data were obtained for this system. The following equations were used to obtain the electromechanical parameters **[38]**:

$$Q_m = \frac{1}{2\pi f_r Z_m C}\left(\frac{{f_a}^2}{{f_a}^2 - {f_r}^2}\right) \tag{4}$$

$$k_p \approx \frac{f_a^2 - f_r^2}{f_a}, \tag{5}$$

$$k_{31} = \sqrt{\frac{\pi}{2}\frac{f_a}{f_r}\frac{1}{\frac{\pi}{2}\frac{f_a}{f_r} - \tan\left(\frac{\pi}{2}\frac{f_a}{f_r}\right)}}, \tag{6}$$

$$s_{11}^E = \frac{1}{4\rho {f_r}^2 w^2}, \tag{7}$$

$$d_{31} = k_{31}\sqrt{\varepsilon\, s_{11}^E}, \tag{8}$$

where, in addition to the parameters (d_{31}, k_p, and Q_m) previously defined, f_r, f_a, Z_m, C, k_{31}, , s_{11}^E, ε, ρ, and w are resonance frequency, anti-resonance frequency, minimum impedance, Capacitance (in Farads), electromechanical coupling factor in the length extensional mode, elastic coefficient at constant electric field, dielectric permittivity at room temperature, density in Kg/m^3, and width of the ceramics, respectively.

4 Discussion

4.1 Structural analysis of BTZ ceramics: from SHS powders to SPS and post-annealed samples. Evolution of their composition

The presence of the high-temperature stable *h* $BaTiO_3$ phase in the SHS product with a small contribution of peaks attributed to *t* BTZ is likely ascribed to the severe processing conditions (high temperature, heating, and cooling rates) inherent to the synthesis process as well as to the reducing environment (Argon gas) correspondingly adopted. The additional *c* $BaZrO_3$ phase is also detected at Zr content ≥ 15 wt.%, i.e. (BTZ015, BTZ020, and BTZ025), proving that a solid solution has not formed between the $BaTiO_3$ and $BaZrO_3$ phases, while a co-existence of the individual phases is obtained. When $x \leq 0.10$, no $BaZrO_3$ phase was detected due to the low concentration of Zr. It should be noted that the detailed quantitative analysis of the XRD pattern (Rietveld method) for the BTZ015 powder also evidenced the presence of a small amount of *c* $BaTiO_3$ along with traces of Ba_2TiO_4 **[30]**. Nonetheless, due to the relatively low intensity of the corresponding peaks, these two phases cannot be unequivocally identified in the XRD patterns shown in **Fig. 1**, so that they are not considered in the present work.

After SPS, a decrease in the *h* $BaTiO_3$ peak intensity is observed with respect to the starting SHS powders. Moreover, according to the Zr content, the *h* $BaTiO_3$ phase is gradually transformed into *t* BTZ or *c* BTZ, as the T_D value is progressively increased. The *c* BTZ phase is favored in particular when the Zr content is in the range x=0.05–0.25 and the sintering temperature is set at 1400ºC (**Fig. 2b**). Twofold effects are noticeable for both the highest Zr content (i.e x=0.25) and the highest sintering temperature (i.e. T_D=1400°C): the formation of the *c* BTZ phase concomitant with the disappearance of the *t* BTZ phase. In parallel, the secondary *c* $BaZrO_3$ phase (c BZ) tends to progressively disappear as the sintering temperature is increased from 1200 to 1400°C. The

overall XRD study shows that the targeted $BaTi_{(1-x)}Zr_xO_3$ solid solution can only be obtained after SHS-SPS under specific conditions of composition and temperature. A high-temperature treatment of the SPS product is required to obtain the targeted single-phase BTZ.

The decisive role of the post-annealing treatment on the evolution of the phases present in SPS ceramics is emphasized here. Beyond its role of re-oxidizing the ceramics, post-annealing, when performed at sufficiently high temperature, allows for the elimination of the *h* $BaTiO_3$ phase still present in some of the SPS ceramics. However, it should be noted that, during the post-annealing process, the hexagonal and tetragonal phases are generally converted into the cubic one. This is in agreement with the work of **[39]** focused on $BaZr_{0.05}Ti_{0.95}O_3$ ceramics obtained by conventional technique, where sintering at higher temperatures caused a transformation from the tetragonal to cubic phase. The formation of the *c* BTZ phase for Zr content corresponding to x=0.10–0.25 is also consistent with similar results reported in the literature for BTZ ceramics obtained by conventional solid-state reactions **[33]**.

Besides, it is clear from the evolution of the secondary *c* $BaZrO_3$ phase as a function of the thermal cycle, that the procedure to eliminate such unwanted secondary phase is to combine SPS sintering at 1400°C with a post-thermal treatment carried out at least at 1200°C (**Fig. 3**).

In addition, whatever the Zr content the post-annealing must be performed at least at 1200°C to efficiently re-oxidize the samples. It is worth noting that an annealing duration of 3h is efficient enough and is much shorter than the one reported in the literature **[23, 27]**.

4.2 Dielectric behavior: Effect of sintering temperature and composition

For a fixed Zr content (x=0.05), a normal ferroelectric behavior is observed. However, for T_D =1400ºC, the Orthorhombic–Tetragonal [O–T] phase transition becomes less marked

compared with ceramics obtained at $T_D \leq 1300$ºC, and a broad transition is observed at T_c. This effect can be correlated with the XRD analysis that shows a transition from *t* BTZ to *c* BTZ, when increasing the sintering temperature. Generally, all BTZ ceramics compositions sintered at T_D =1200ºC, showed a normal ferroelectric behavior except for the composition corresponding to x=0.25. In the latter case, the very diffuse phase transition associated with low permittivity values is correlated with the low value of density obtained at 1200°C. The microstructural investigation of BTZ025 sintered at 1200°C confirms a poorly densified ceramic and the presence of cracks. It is worth noting that no significant shift in $T_{O\text{-}T}$ and T_c was observed from x= 0.05 to x= 0.20, thus demonstrating that a sintering temperature of 1200°C is not sufficient to induce the Zr-Ti substitution.

When sintering is performed at 1400°C, a continuous decrease of T_c is observed when the composition was varied from x=0.10 to x=0.25 and the transition becomes more and more diffuse. A relaxor behavior starts to be detected for x=0.25 (ΔTm = 8 from 100 Hz to 500 kHz), for which *c* BTZ is the only phase observed on the room temperature XRD pattern (**Fig. 3(c)**).

As a result, a change from classical to diffuse ferroelectric behavior in SHS-SPS ceramics can be induced by increasing not only the Zr content but also the sintering temperature at a fixed composition. Considering the microstructural analysis, such dielectric behavior is not correlated to the microstructure, while, as expected, depends rather on compositional effects at the atomic scale.

High diffusivity parameter (γ) was observed at low Zr content. The reason for this finding could be related to the coexistence of tetragonal and cubic phases seen in **Fig. 3(b)**. However, at high Zr content, the obtained γ parameter is in the range of the values reported in the literature, which generally depend on the adopted synthesis process **[32, 40-41]**. In addition, similar to the

works by **[42]** and **[20],** higher sintering temperature induces diffuse transition and increases the γ parameter (**Table S2, Suppl. material**). The T_c (T_m) values obtained for the various compositions are in good agreement with the literature for BTZ ceramics obtained by other methods **[43-45]**.

4.3 Piezoelectric study

Both the composition and the sintering temperature have an impact on the piezoelectric performances. The piezoelectric charge coefficient decreases with increasing *x* values (**Fig. 10(a)**), which confirms that high Zr content does not favor the obtainment of good piezoelectric properties. This result is effectively in agreement with the improved piezoelectric properties reported for BTZ ceramics with $x \leq 0.08$ **[44, 46]**. In addition, our study also evidenced that, when operating under optimal SPS temperature (T_D) conditions to obtain higher values of the dielectric permittivity, the piezoelectric properties are correspondingly enhanced, which is in line with results reported in the literature for BTZ ceramics produced by alternative techniques **[46-47]**.

When considering BTZ005, sintering at 1200°C results in moderate density values and poor quality of grain boundaries, that are not convenient for improving piezoelectric properties. On the other hand, BTZ005 sintered at 1300°C exhibits the optimal piezoelectric properties, which is in agreement with the literature **[36-37, 48]**. However, the obtained piezoelectric coefficient remains relatively low when compared to the state of the art **[23, 44, 48]**. Improvements based on microstructure (density and grain size) and on the poling conditions would allow reaching better performances.

5. Conclusion

BTZ ceramics have gained a high interest due to the possibility to tailor their ferroelectric properties through the control of composition. Different BTZ ceramics are produced in this work using a novel approach based on the combination of the fast SHS and SPS processes, followed by an air-thermal treatment of relatively short duration (3h), compared to the annealing time (10 h) typically considered in the literature. Here, the possibility of tuning the dielectric response (from classical to diffuse phase transition or relaxor) by varying, for a given composition, the sintering temperature, was clearly evidenced. In this regard, it should be noted that, to the best of our knowledge, no study was reported so far in the literature on the influence of the SPS temperature on the dielectric behavior of BTZ ceramics, regardless of the method used for powder synthesis.

Specifically, it was observed that the T_D value and the Zr content significantly impact the structure, microstructure, dielectric, and piezoelectric properties of the SHS-SPS prepared ceramics. The $BaZrO_3$ impurity phase formed during SHS, and still present after SPS, was eliminated thanks to the post-annealing treatment of the sintered ceramics. Increasing the sintering temperature above 1200°C leads to improved density, more homogeneous microstructure, as well as enhanced dielectric permittivity. The ceramic containing 5 at.% of Zr sintered at T_D=1300ºC showed the best piezoelectric properties. Better performances are expected if a single-phase ceramic is obtained after SPS and the microstructure of the final ceramics is suitably refined. Work is underway along this direction.

Acknowledgments

One of the authors (B.N.E) performed her activity in the framework of the International PhD in Innovation Sciences and Technologies at the University of Cagliari and is also grateful for the ERASMUS Placedoc program for allowing mobility to France.

References

[1] J.Z. Jiang, F.W. Poulsen, S. Mørup, Structure and thermal stability of nanostructured iron doped zirconia prepared by high-energy ball milling. J. Mat. Res. 14(1999)1343–1352. https://doi.org/10.1557/JMR.1999.0183.

[2] R. Potong, R. Rianyoi, A. Chaipanich, Dielectric Properties of Lead-Free Composites from 0-3 Barium Zirconate Titanate-Portland Cement Composites. Ferro. Lett. Sec., 38(2011) 18–23. https://doi.org/10.1080/07315171.2011.570176.

[3] R. Saravanan, Titanate based ceramic dielectric material, first ed., Materials research forum, Millersville, USA, 2018, pp 10. https://doi.org/10.21741/9781945291555.

[4] U. Ahmadu, A. Muazu, S. Umar, Physical properties of porous pure and Zr/Sn-doped nanocrystalline $BaTiO_3$ ceramics, in: U.M. Basheer Al-Naib (Ed.), Recent Advances. Porous Ceramics, IntechOpen Ltd, London, UK, 2018, pp. 147–170. https://doi.org/10.5772/intechopen.75500.

[5] B. Garbarz-Glos, K. Bormanis, D. Sitko, Effect of Zr Doping on the Electrical Properties of $BaTiO_3$ Ceramics. Ferro. 417(2011)118–123. https://doi.org/10.1080/00150193.2011.578508.

[6] T. Maiti, R. Guo, A.S. Bhalla, Evaluation of experimental resume of $BaZr_xTi_{1-x}O_3$ with perspective to ferroelectric relaxor family: An overview. Ferro., 425(2011)4–26. https://doi.org/10.1080/00150193.2011.644168.

[7] T. Maiti, R. Guo, A.S. Bhalla, Structure-Property Phase Diagram of $BaZr_xTi_{1-x}O_3$ System, J. Am. Ceram. Soc., 91(2008)1769–1780. https://doi.org/10.1111/j.1551-2916.2008.02442.x.

[8] N. Nanakorn, P. Jalupoom, N. Vaneesorn, A. Thanaboonsombut, Dielectric and ferroelectric properties of $Ba(Zr_xTi_{1-x})O_3$ ceramics. Ceram. Int., 34(2008)779–782. https://doi.org/10.1016/j.ceramint.2007.09.024.

[9] S.J. Kuang, X.G. Tang, L.Y. Li, Y.P. Jiang, Q.X. Liu, Influence of Zr dopant on the dielectric properties and Curie temperatures of $Ba(Zr_xTi_{1-x})O_3$ ($0 \leq x \leq 0.12$) ceramics. Scrip. Mat. 61(2009)68–71. https://doi.org/10.1016/j.scriptamat.2009.03.016.

[10] T. Maiti, R. Guo, R., A. S. Bhalla, 2007. Enhanced electric field tunable dielectric properties of $BaZr_xTi_{1-x}O_3$ relaxor ferroelectrics. Appl. Phys. Lett. 90, 182901. https://doi.org/10.1063/1.2734922.

[11] P.S. Dobal, A. Dixit, R.S. Katiyara, Z. Yu, R. Guo, A.S. Bhalla, Micro-Raman scattering and dielectric investigations of phase transition behavior in the $BaTiO_3$–$BaZrO_3$ system. J. Appl. Phys. 89(2001)8085-8091. https://doi.org/10.1063/1.1369399.

[12] D. Hennings, A. Schnell, G. Simon, Diffuse Ferroelectric Phase Transitions in $Ba(Ti_{1-y}Zr_y)O_3$ Ceramics. J. Am. Ceram Soc., 65(1982) 539–544. https://doi.org/10.1111/j.1151-2916.1982.tb10778.x.

[13] J. Ravez, A. Simon, Temperature and Frequency Dielectric Response of Ferroelectric Ceramics with Composition $Ba(Ti_{1-x}Zr_x)O_3$. Eur. J. Sol. Inorg Chem. 34(1997), 1199–1209.

[14] M.H. Frey D.A. Payne, Grain-size effect on structure and phase transformations for barium titanate. Phys. Rev. B 54 (1996) 3158–3168. https://doi.org/10.1103/PhysRevB.54.3158.

[15] T.T. Fang, H.-L. Hsieh, F.-S. Shiau, Effects of Pore Morphology and Grain Size on the Dielectric Properties and Tetragonal–Cubic Phase Transition of High-Purity Barium

Titanate. J. Am. Ceram Soc., 76(1993)1205–1211. https://doi.org/10.1111/j.1151-2916.1993.tb03742.x.

[16] X.G. Tang, J. Wang, X.X. Wang, H.L.W. Chan, Effects of grain size on the dielectric properties and tunabilities of sol–gel derived $Ba(Zr_{0.2}Ti_{0.8})O_3$ ceramics. Sol. Comm. 131 (2004)163–168. https://doi.org/10.1016/j.ssc.2004.05.016.

[17] M. Aghayan, A.K. Zak, M. Behdani, A.M. Hashim, Sol–gel combustion synthesis of Zr-doped $BaTiO_3$ nanopowders and ceramics: dielectric and ferroelectric studies, Ceram. Int. 40 (2014)16141−16146. https://doi.org/10.1016/j.ceramint.2014.07.045.

[18] M. Deluca, C.A. Vasilescu, A.C. Ianculescu, D.C. Berger, C.E. Ciomaga, L.P. Curecheriu, L. Stoleriu, A. Gajovic, L. Mitoseriu, C. Galassi, Investigation of the composition-dependent properties of $BaTi_{1-x}Zr_xO_3$ ceramics prepared by the modified Pechini method, J. Eur. Ceram. Soc. 32(2012)3551–3566. http://dx.doi.org/10.1016/j.jeurceramsoc.2012.05.007.

[19] T. Badapanda, S. Chaterjee, A. Mishra, R. Ranjan, S. Anward, Electric field induced strain, switching and energy storage behaviour of lead free barium zirconium titanate ceramic, Phys. B 521(2017)264–269. https://doi.org/10.1016/j.physb.2017.07.013.

[20] M.L.V. Mahesh, V.V.B. Prasad, A.R. James, Effect of sintering temperature on the microstructure and electrical properties of zirconium doped barium titanate ceramics, *J* Mat. Sci: Mat. Electron 24(2013)4684–4692. https://doi.org/10.1007/s10854-013-1460−3.

[21] P. Julphunthong, T. Bongkarn, Phase formation, microstructure and dielectric properties of $Ba(Zr_{0.1}Ti_{0.9})O_3$ ceramics prepared via the combustion technique. Cur. Appl. Phys. 11 (2011)S60−S65.

[22] A. Ahmad, K.A. Razak, 2017. Synthesis of $BaTiO_3$ and $Ba(Zr_xTi_{1-x})O_3$ by using the soft combustion method. AIP Conf. Proc. 1865, 060001. https://doi.org/doi: 10.1063/1.4993377.

[23] H. Maiwa, Electromechanical properties of $Ba(Zr_{0.2}Ti_{0.8})O_3$ ceramics prepared by spark plasma sintering. Ceram. Int 38(2012)S219-S223. https://doi.org/10.1016/j.ceramint.2011.04.087.

[24] G. Philippot, M. Albino, U.-C. Chung, M. Josse, C. Elissalde, M. Maglione, C. Aymonier, Continuous $BaTi_{1-y}Zr_yO_3$ ($0 \leq y \leq 1$) nanocrystals synthesis in supercritical fluids for nanostructured lead-free ferroelectric ceramics. Mat. Des. 86(2015)354–360. https://doi.org/10.1016/j.matdes.2015.07.111.

[25] B. Liu, Y. Wu, Y.H. Huang, K. X. Song, Y.J. Wu, Enhanced dielectric strength and energy storage density in $BaTi_{0.7}Zr_{0.3}O_3$ ceramics via spark plasma sintering, J Mater Sci. 54(2019)4511–4517. https://doi.org/10.1007/s10853-018-3170-y.

[26] R. Orrù, R. Licheri, A.M. Locci, A. Cincotti, G. Cao, Consolidation/synthesis of materials by electric current activated/assisted sintering. Mater. Sci. Eng. R 63(2009)127–287. https://doi.org/10.1016/j.mser.2008.09.003.

[27] H. Maiwa, Dielectric and Electromechanical Properties of $Ba(Zr_xTi_{1-x})O_3$ (x = 0.1 and 0.2) Ceramics Prepared by Spark Plasma Sintering, Jap. J. Appl. Phys.46(2007)7013–7017. https://doi.org/10.1143/JJAP.46.7013.

[28] A. Varma, A.S. Rogachev, A.S. Mukasyan, S. Hwang, Combustion Synthesis of Advanced Materials: Principles and Applications. Adv. Chem. Eng. 24(1998)79–226. https://doi.org/10.1016/S0065-2377(08)60093-9.

[29] A. Cincotti, R. Licheri, A.M. Locci, R. Orrù, G. Cao, A review on combustion synthesis of novel materials: Recent experimental and modeling results. J. Chem. Tech. Biot. 78(2003)122–127. https://doi.org/10.1002/jctb.757.

[30] B.N. Ezealigo, R. Orrù, F. Torre, P.C. Ricci, F. Delogu, G. Cao, Annealing effects on the structural and optical properties of undoped and Zr-doped Ba titanate prepared by self-propagating high-temperature synthesis. Ceram. Int. 46(11) (2020) 17307-17314. https://doi.org/10.1016/j.ceramint.2020.04.019.

[31] N. Sawangwan, J. Barrel, K. Mackenzie, T. Tunkasiri, The Effect of Zr Content on Electrical Properties of $Ba(Ti_{1-X}Zr_x)O_3$ Ceramics. Appl. Phys. A 90(2008)723–727. https://doi.org/10.1007/s00339-007-4342-9.

[32] S. Mahajan, O.P. Thakur, C. Prakash, K. Sreenivas, Effect of Zr on dielectric, ferroelectric and impedance properties of $BaTiO_3$ ceramic. Bull Mat. Sci., 34(2011)1483–1489. https://doi.org/10.1007/s12034-011-0347-2.

[33] P. Sateesh, J. Omprakash, G.S. Kumar, G. S., G. Prasad, 2015. Studies of phase transition and impedance behavior of Ba(Zr, Ti) O_3 ceramics, *J. Adv. Dielectrics,* 5, 1550002. https://doi.org/ 10.1142/S2010135X15500022.

[34] F. Benaballah, A. Simon, H. Khemakhem, C. Elissalde, M. Maglione, 2011. Linking large piezoelectric coefficients to highly flexible polarization of lead free $BaTiO_3$-$CaTiO_3$-$BaZrO_3$ ceramics. J. Appl. Phys. 109, 124116. https://doi.org/10.1063/1.3599854.

[35] C.A. Schneider, W.S Rasband, K.W. Eliceiri, NIH Image to Image J: 25 years of image analysis. Nat. methods 9(7) (2012)671-675. https://doi.org/doi: 10.1038/nmeth.2089.

[36] Z. Yu, C. Ang, R. Guo, A.S. Bhalla, Piezoelectric and strain properties of $Ba(Ti_{1-x}Zr_x)O_3$ ceramics. J. Appl. Phys. 92(2002)1489–1493. https://doi.org/10.1063/1.1487435.

[37] P. Zheng, J.L. Zhang, S.F. Shao, Y.Q. Tan, C.L. Wang, Piezoelectric properties and stabilities of CuO-modified ceramics. Appl. Phys. Lett. 94(2009)032902. https://doi.org/10.1063/1.3072347.

[38] T.L. Jordan and Z. Ounaies, Piezoelectric Ceramics Characterization, NASA, Langley Research Center Hampton, Virginia, 2001, https://apps.dtic.mil/dtic/tr/fulltext/u2/a395517.pdf

[39] P.A. Jha A.K. Jha, Effect of sintering temperature on the grain growth and electrical properties of barium zirconate titanate ferroelectric ceramics. J Mat. Sci: Mat. Electron 24(2013)1511–1518. https://doi.org/10.1007/s10854-012-0963-7.

[40] Z. Sun, Y. Pun, Z. Dong, Y. Hu, X. Liu, P. Wang, Effect of Zr^{4+}content on the T_C range and dielectric and ferroelectric properties of $BaZr_xTi_{1-x}O_3$ ceramics prepared by microwave sintering. Ceram. Int. 40(2014)3589–3594, http://dx.doi.org/10.1016/j.ceramint.2013.09.069.

[41] C. Fu, F. Pan, W. Cai, X. Deng, X. Liu, 2009. Microstructures and dielectric properties of $BaZr_{0.2}Ti_{0.8}O_3$ ceramics. J Phys. Conf. Ser. 152, 012075. https://doi.org/10.1088/1742-6596/152/1/012075.

[42] W. Cai, J. Gao, M. Zhang, C. Fu, Effect of sintering temperature on diffuse phase transition of barium zirconate titanate ceramics. Int. Ferro. 105(2009)1−10. https://doi.org/10.1080/10584580903034548.

[43] Z. Yu, R. Guo, A.S. Bhalla, Dielectric behavior of $Ba(Ti_{1-x}Zr_x)O_3$ single crystals, J. Appl. Phys. 88 (2000)410−415. https://doi.org/10.1063/1.373674.

[44] L. Dong, D.S. Stone, R.S. Lakes, Enhanced dielectric and piezoelectric properties of $_xBaZrO_3$-(1-x)$BaTiO_3$ ceramics, 2012. J Appl. Phys. 111, 084107 http://dx.doi.org/10.1063/1.4705467.

[45] F. Moura, A.Z. Sim˜oes, B.D. Stojanovic, M.A. Zaghete, E. Longo, J.A.Varela, Dielectric and ferroelectric characteristics of barium zirconate titanate ceramics prepared from mixed

oxide method, J. Alloys and Compds 462(2008)129–134. http://dx.doi.org/10.1016/j.jallcom.2007.07.077.

[46] A.K. Kalyani, K. Brajesh, A. Senyshyn, R. Ranjan, 2014. Orthorhombic-tetragonal phase coexistence and enhanced piezo-response at room temperature in Zr, Sn, and Hf modified $BaTiO_3$. Appl. Phys. Lett. 104, 252906. https://doi.org/10.1063/1.4885516.

[47] S.-J. Jeong, D.-S. Lee, E.-C. Park, J.-S. Song, Piezoelectric properties of a $Ba(Zr_{0.075}Ti_{0.925})O_3$ single crystal induced by poling treatment. J Electroceram, 17 2006)537–541. https://doi.org/10.1007/s10832-006-7724-z.

[48] W. Li, Z. Xu, R. Chu, P. Fu, G. Zang, Dielectric and piezoelectric properties of $Ba(Zr_xTi_{1-x})O_3$ lead-free ceramics. Braz. J. Phys. 40(2010)353–356. http://dx.doi.org/10.1590/S0103-97332010000300018.

Figures

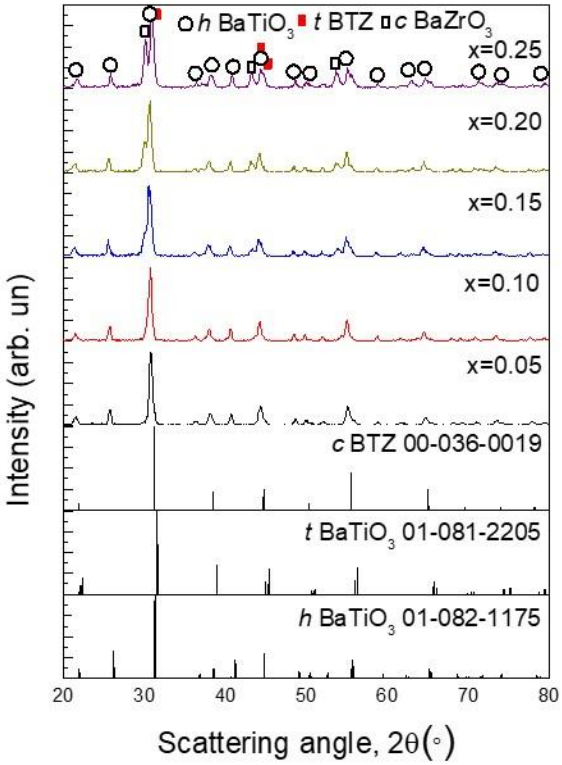

Figure 1: Room temperature XRD patterns of powders obtained by SHS for different *x* values (0.05-0.25) in Eq. (1).

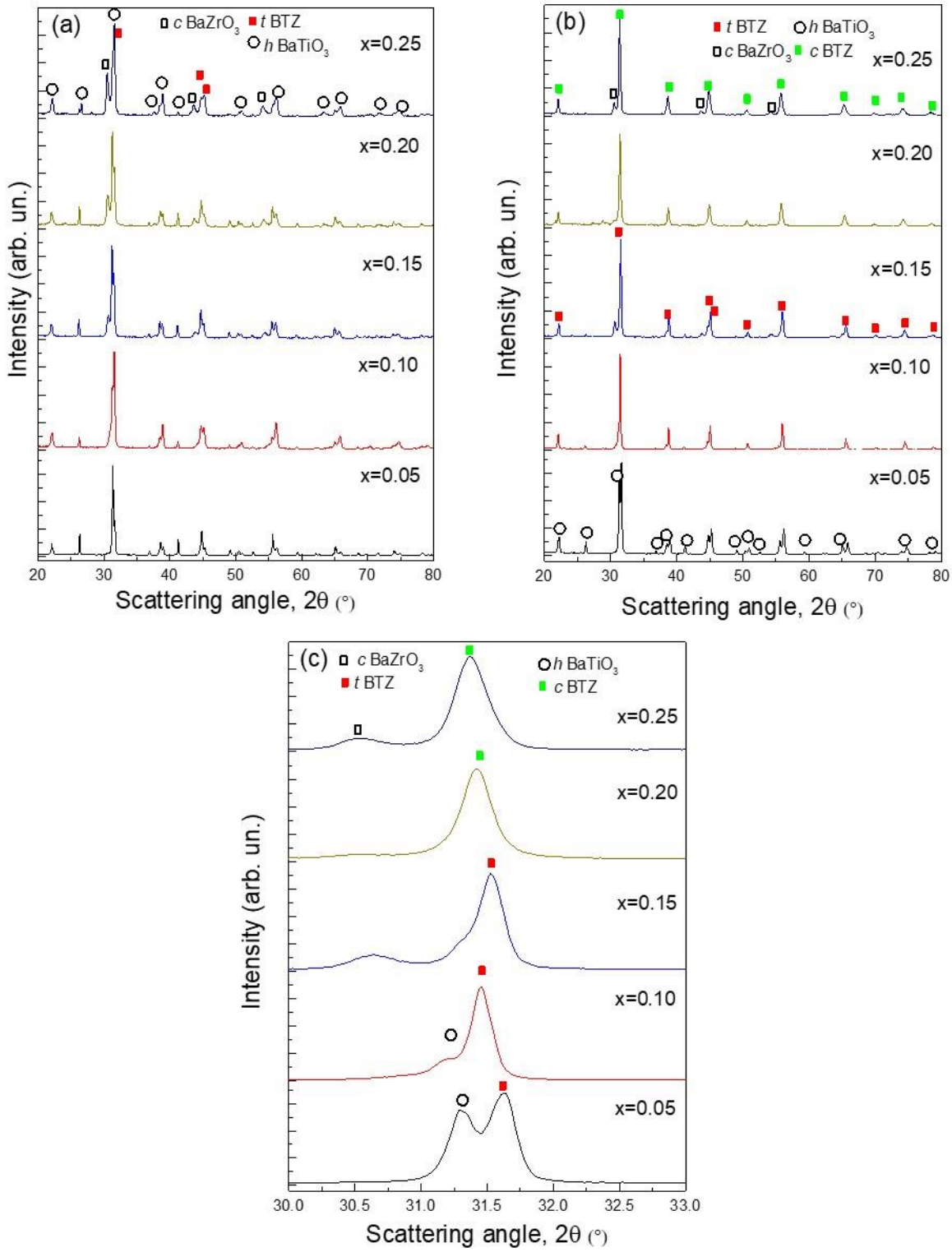

Figure 2: XRD patterns of BTZ ceramics obtained by SPS at (a) T_D= 1200ºC, (b) T_D= 1400°C, (c) Zoomed view of (b).

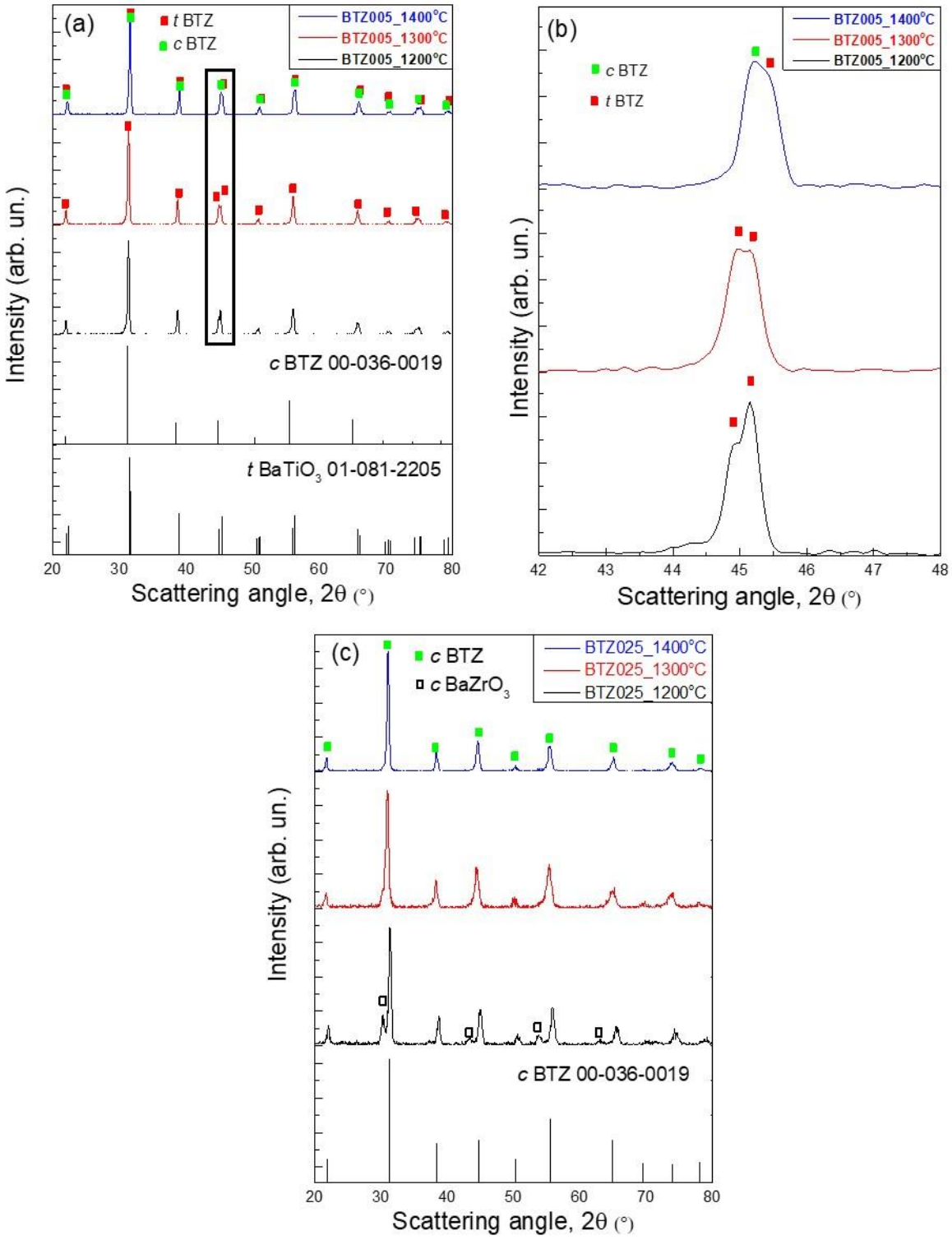

Figure 3: XRD patterns of (a)-(b) BTZ005, (c) BTZ025 ceramics obtained by SPS (T_D=1200, 1300, and 1400°C) after being post annealed for 3h at 1200°C.

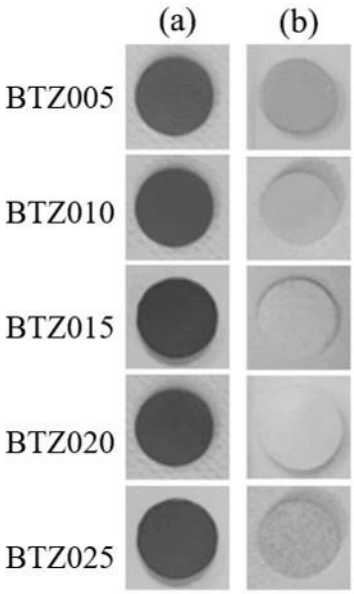

Figure 4: Images of $BaTi_{(1-x)}Zr_xO_3$ *(x=0.05–0.25)* ceramics sintered by SPS at 1400°C before (a) and after (b) post-annealing at 1200°C for 3h.

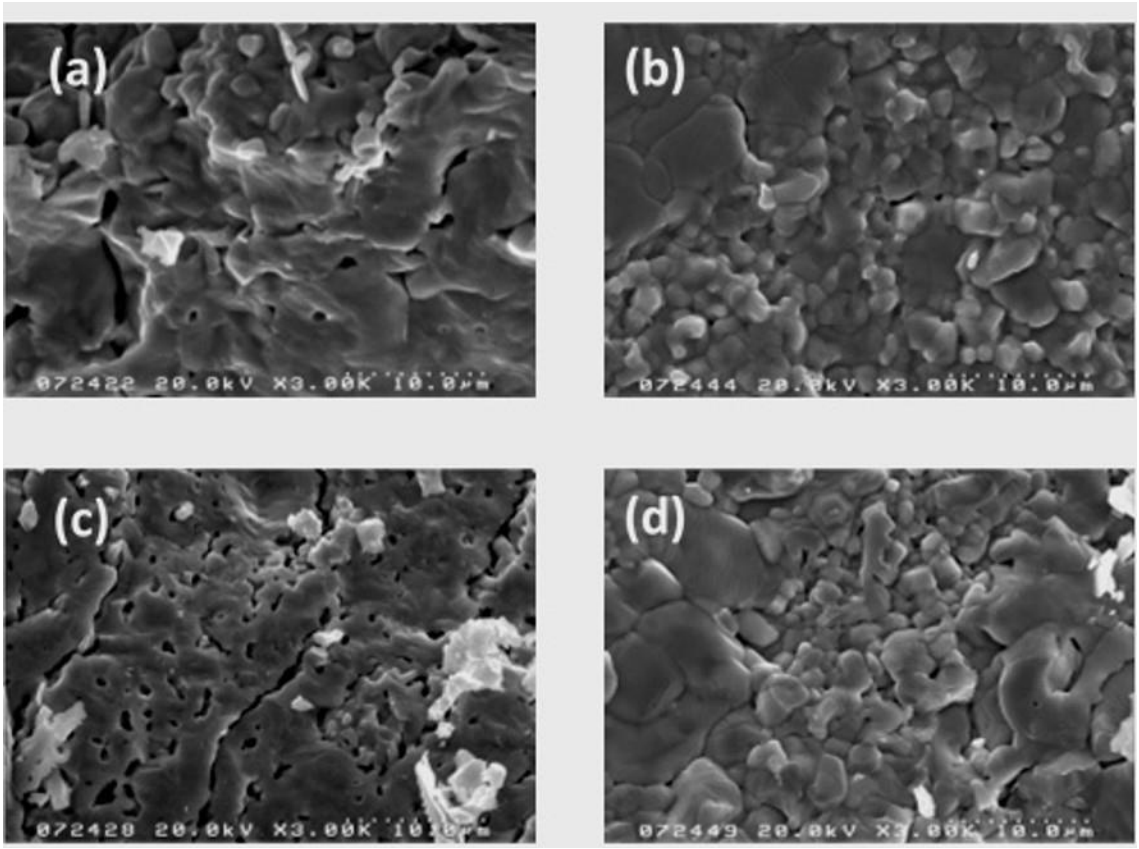

Figure 5: Fractured surfaces of BTZ ceramics obtained by SPS and subsequently annealed at 1200ºC for 3h: (a) BTZ005, T_D=1200°C; (b) BTZ005, T_D=1400°C; (c) BTZ025, T_D=1200°C; (d) BTZ025, T_D=1400°C.

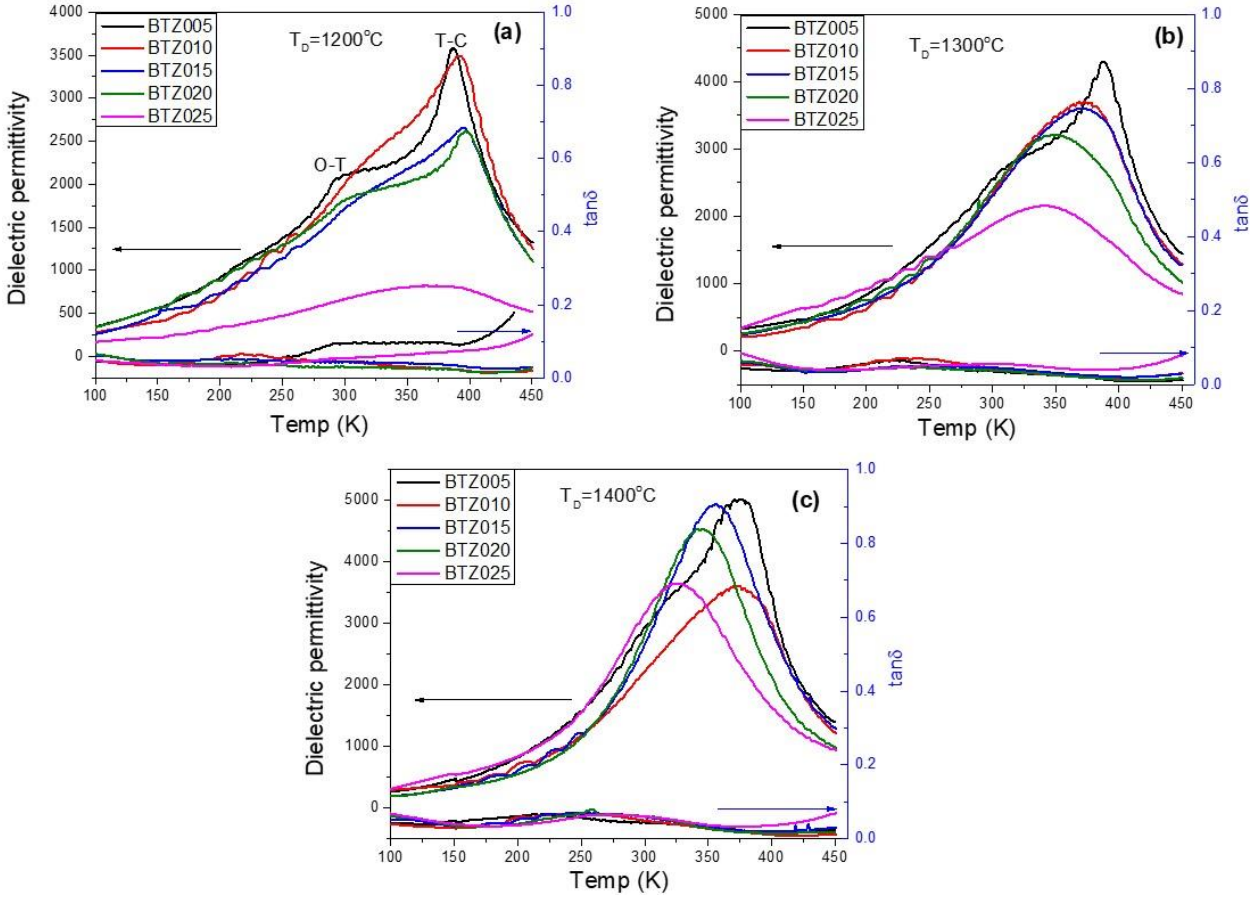

Figure 6: Dielectric permittivity and loss of $BaTi_{(1-x)}Zr_xO_3$ *(x=0.05–0.25)* ceramics at 1KHz for (a) T_D=1200°C (b) T_D=1300°C (c) T_D=1400°C. (O= orthorhombic; T= tetragonal; C=cubic phase transition; all samples were post-annealed for 3h at 1200ºC).

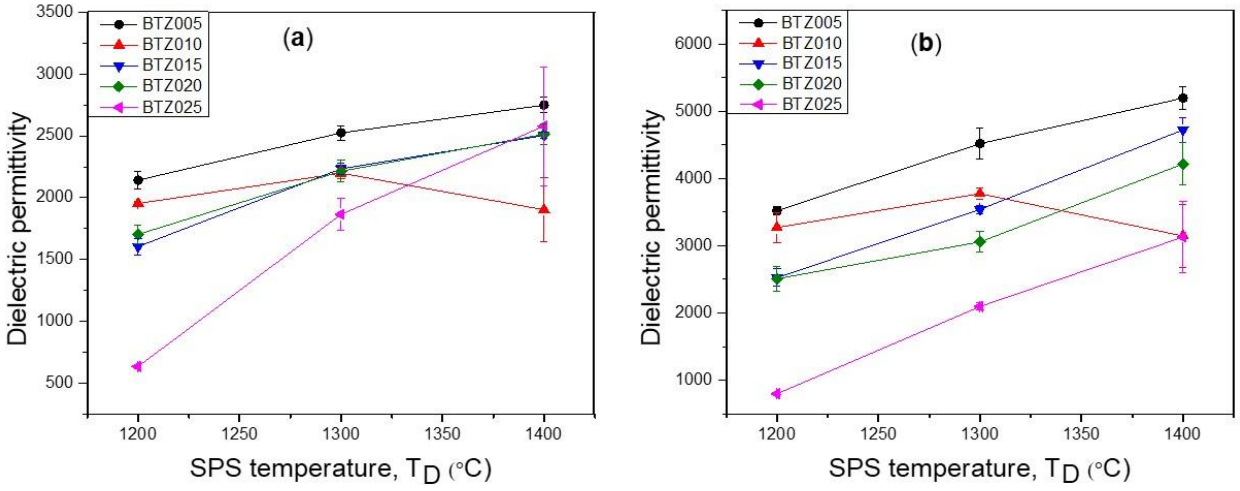

Figure 7: Dielectric permittivity of $BaTi_{(1-x)}Zr_xO_3$ *(x=0.05–0.25)* ceramics as a function of SPS temperature (a) at room (25ºC) and (b) at Curie (T_c) temperature, respectively.

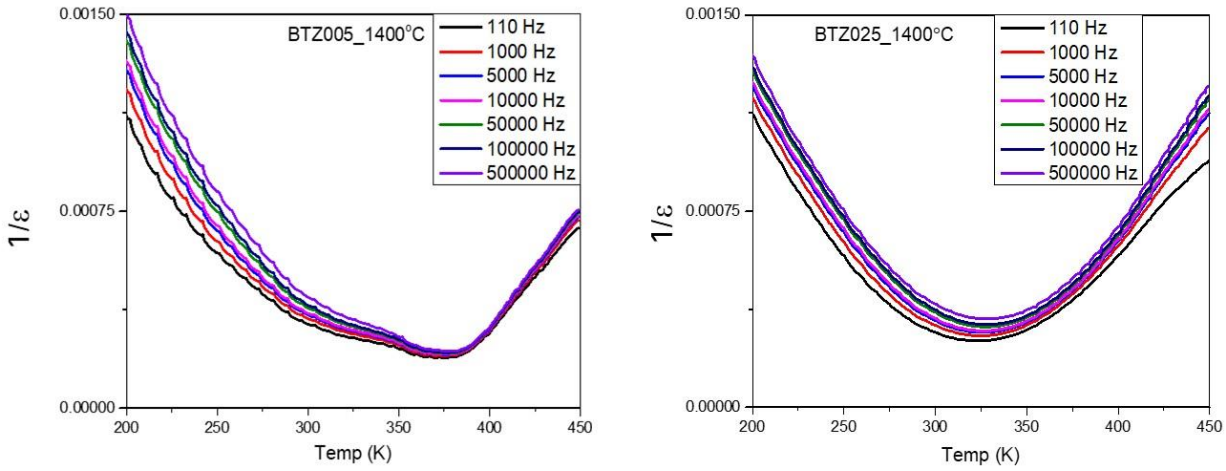

Figure 8: Curie-Weiss plots of $BaTi_{(1-x)}Zr_xO_3$ *(x=0.05 and 0.25)* ceramics sintered at 1400°C and subsequently post-annealed at 1200°C for 3h.

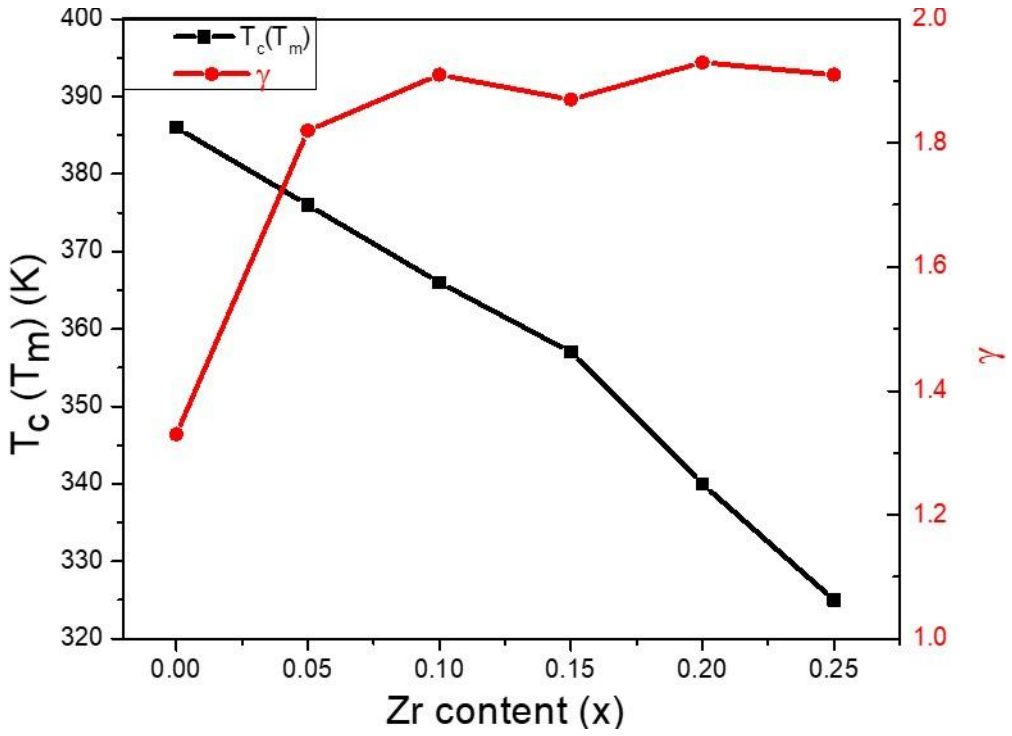

Figure 9: Plot of T_c (T_m) at 1 kHz and diffuseness coefficient (γ) as a function of Zr content for ceramics sintered at 1400°C and subsequently post-annealed at 1200°C for 3h.

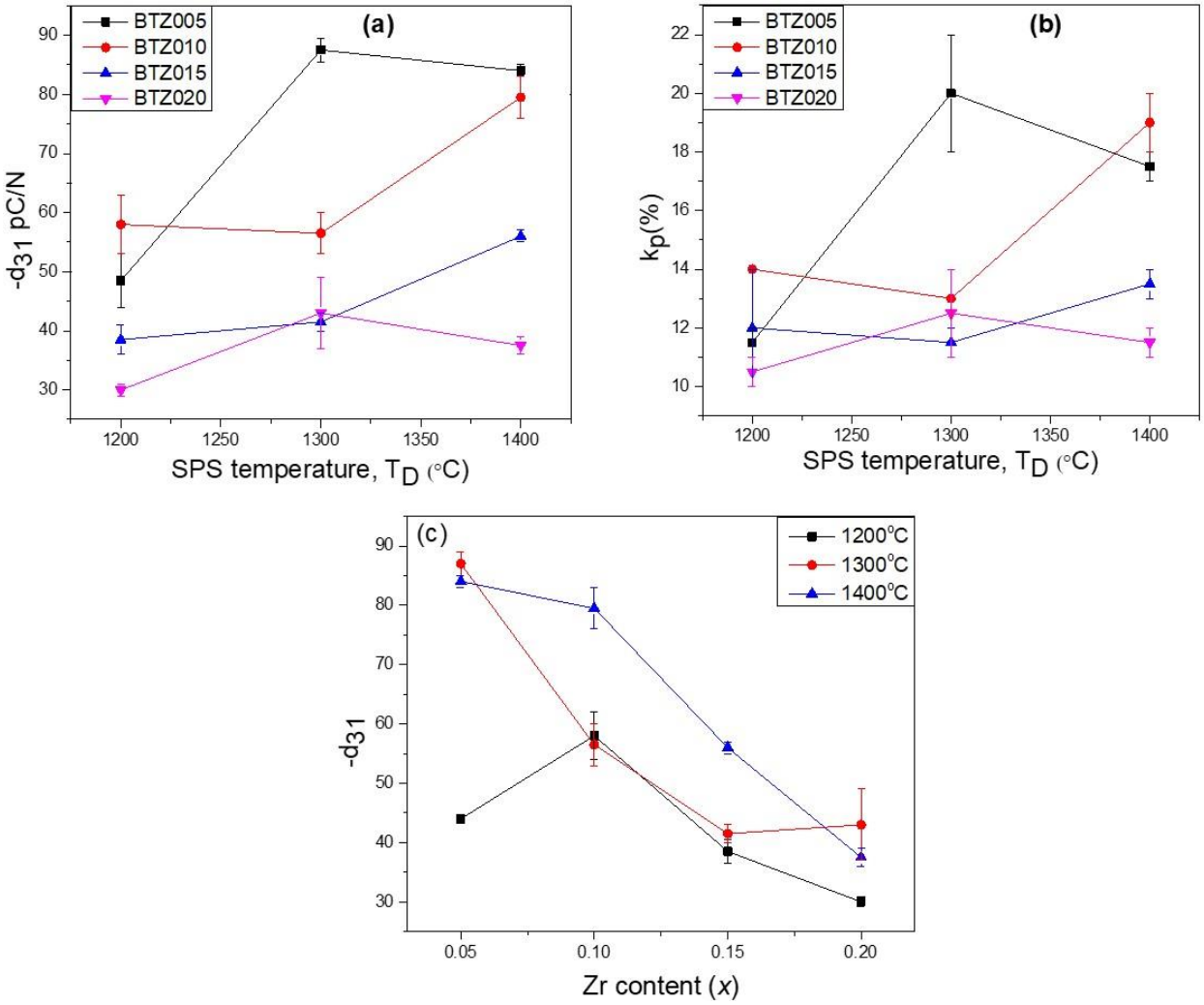

Figure 10: Piezoelectric properties of BTZ ceramics annealed at 1200ºC for 3h. **(a)** Piezoelectric charge coefficient (d_{31}) and **(b)** planar coupling factor (k_p) as a function of sintering temperature; **(c)** Piezoelectric charge coefficient (d_{31}) as a function of Zr content.